Preclinical Evaluation of ^{18}F-PF-05270430, a Novel PET Radioligand for the Phosphodiesterase 2A Enzyme

Authors: Laigao Chen[1]*, Nabeel Nabulsi[2]*, Mika Naganawa[2], Kenneth Zasadny[1], Marc B. Skaddan[1], Lei Zhang[3], Soheila Najafzadeh[2], Shu-fei Lin[2], Christopher J. Helal[1], Tracey L. Boyden[1], Cheng Chang[1], Jim Ropchan[2], Richard E. Carson[2], Anabella Villalobos[1], Yiyun Huang[2]

[1]Pfizer Worldwide Research and Development, Eastern Point Road, Groton, CT 06340, USA

[2]PET Center, Department of Radiology and Biomedical Imaging, Yale University, New Haven, CT 06520, USA

*Co-first authors

Corresponding Author:

Yiyun Huang, PET Center, Yale University School of Medicine, New Haven, CT 06520, USA;

henry.huang@yale.edu

First Authors:

Laigao Chen, Pfizer Worldwide Research and Development, Eastern Point Road, Groton, CT 06340, USA; laigao.chen@pfizer.com

Nabeel Nabulsi, PET Center, Yale University School of Medicine, New Haven, CT 06520, USA; nabeel.nabulsi@yale.edu

Financial support

Word count: 4988

Running Title: Preclinical Study of Novel PDE2A Tracer

The enzyme phosphodiesterase 2A (PDE2A) is a potential target for development of novel therapeutic agents for the treatment of cognitive impairments. The goal of the present study was to evaluate the PDE2A ligand ^{18}F-PF-0150270430, 4-(3-fluoroazetidin-1-yl)-7-methyl-5-(1-methyl-5-(4-(trifluoromethyl)phenyl)-1H-pyrazol-4-yl)imidazo[1,5-f][1,2,4]triazine, in nonhuman primates.

Methods: ^{18}F-PF-05270430 was radiolabeled by two methods via nucleophilic substitution of its tosylate precursor. Tissue metabolite analysis in rodents and positron emission tomography (PET) imaging in non-human primates under baseline and blocking conditions were performed to determine the pharmacokinetic and binding characteristics of the new radioligand. Various kinetic modeling approaches were assessed to select the optimal method for analysis of imaging data.

Results: ^{18}F-PF-05270430 was synthesized in >98% radiochemical purity and high specific activity. In the non-human primate brain, uptake of ^{18}F-PF-05270430 was fast, with peak concentration (standardized uptake values of 1.5-1.8 in rhesus monkeys) achieved within 7 min after injection. The rank order of uptake was striatum > neocortical regions > cerebellum. Regional time-activity curves were well fitted by the two-tissue (2T) compartment model and the multilinear analysis-1 (MA1) method to arrive at reliable estimates of regional distribution volume (V_T) and binding potential (BP_{ND}) with 120 min of scan data. Regional V_T values (MA1) ranged from 1.28 in the cerebellum to 3.71 in the putamen, with BP_{ND} of 0.25 in the temporal cortex and 1.92 in the putamen. Regional BP_{ND} values estimated by the simplified reference tissue model (SRTM) were similar to those from MA1. Test-retest variability in high binding regions (striatum) was $4 \pm 6\%$ for MA1 V_T, $13 \pm 6\%$ for MA1 BP_{ND}, and $13 \pm 7\%$ for SRTM BP_{ND}, respectively. Pretreatment of animals with the PDE2A inhibitor PF-05180999 resulted in a dose-dependent reduction of ^{18}F-PF-05270430 specific binding, with EC_{50} of 69.4 ng/mL in plasma PF-05180999 concentration.

Conclusion: ^{18}F-PF-05270430 displayed fast and reversible kinetics in non-human primates, as well as specific binding blockable by a PDE2A inhibitor. This is the first PET tracer with desirable imaging properties and demonstrated ability to image and quantify PDE2A in vivo.

Key Words: Phosphodiesterase 2A, Positron Emission Tomography, Radioligand, Non-Human Primates

Schizophrenia is a chronic, highly debilitating psychiatric disorder (*1*). This disease displays positive symptoms (hallucinations, paranoia, delusions), negative symptoms (apathy, alogia, affective flattening), and cognitive symptoms (deficits in memory, attention, and executive function) (*2*). Up to 75% of schizophrenic patients suffer from cognitive impairment (*3*), whose treatment remains a critical unmet medical need, as current antipsychotics most effectively alleviate positive symptoms, modestly improve negative symptoms, but have little to no effect on cognitive deficits (*4,5*). The phosphodiesterase 2A (PDE2A) is a dual-substrate enzyme with highest levels of expression within the limbic and basal ganglia brain circuitry found to be dysfunctional in schizophrenia, and thus has been proposed as a target for drug development for this disorder (*6,7*).

PDE2A protein expression is prominent in the cortex, hippocampus, subiculum, amygdala, caudate, putamen, nucleus accumbens and ventral tegmental areas, and is similarly distributed across rodents, dogs, non-human primates and humans (*6*). PDE2A is concentrated within the synaptic compartments of many glutamatergic structures and thereby potentially positioned to selectively modulate the cyclic nucleotide signaling cascades regulating neurotransmission within the brain circuits involved in schizophrenia (*8*). Dysfunction of the N-methyl-D-aspartate (NMDA) glutamatergic system has been implicated in the pathogenesis of schizophrenia, as NMDA antagonists (e.g. ketamine) reproduce in healthy subjects the symptoms of schizophrenia, including cognitive impairment and negative symptoms (*9*). PDE2A inhibitors have been shown to increase cyclic nucleotide levels in vitro, to enhance long-term potentiation, a measure of synaptic plasticity, in hippocampal slices, and to improve learning and memory in vivo (*10*). Taken together, these findings suggest that PDE2A inhibitors could positively impact cognitive endpoints in schizophrenia.

We have previously reported a novel series of PDE2A inhibitors (*11*). As part of the development program we sought to unequivocally establish the ability of key compounds to permeate the blood-brain barrier and bind to PDE2A to potentially serve as therapeutics for cognitive impairment associated with schizophrenia. One way to do this is by developing a PDE2A positron emission tomography (PET) ligand for use in the assessment of drug candidates via target occupancy studies. So far there has been only one report of attempt to develop PET imaging agents for PDE2A, but no suitable radioligand was found (*12*). We have previously defined a set of selection criteria for novel radiotracers for the central nervous system (CNS) through a systematic analysis of physicochemical properties of validated PET ligands (*13*). Application of these criteria to our PDE2A inhibitor library led to the identification of PF-05270430, 4-(3-fluoroazetidin-1-yl)-7-methyl-5-(1-methyl-5-(4-(trifluoromethyl)phenyl)-1H-pyrazol-4-yl)imidazo[1,5-f][1,2,4]triazine (Fig. 1), as a promising tracer candidate. In addition to its sub-nanomolar affinity to PDE2A enzyme (IC_{50} = 0.53 nM) and exquisite selectivity over other PDEs and a broad panel of CNS targets (all < 30% inhibition at 1 μM), PF-05270430 fits our defined favorable PET property space nicely (See Supplemental Table S1). In this paper we report the radiosynthesis of ^{18}F-PF-05270430 as the first PET radioligand for PDE2A, its radioactive metabolite profiles in both rats and non-human primates (NHP), and imaging evaluation in non-human primates (NHP). The companion paper reports the tracer's radiation dosimetry in NHP, toxicology data summary, safety, tolerability and test/retest reproducibility evaluation in healthy human subjects (*14*).

MATERIAL AND METHODS

All experiments involving laboratory animals were carried out in accordance with federal, state, local and institutional guidelines governing the use of laboratory animals in

research, and were reviewed and approved by Institutional Animal Care and Use Committee at Pfizer and Yale University.

Synthesis of PF-05270430 and the radiolabeling precursor for ^{18}F-PF-05270430

Synthesis of PF-05270430 and the tosylate radiolabeling precursor were prepared according to procedures reported previously (*13*).

Radiosynthesis of ^{18}F-PF-05270430

^{18}F-PF-05270430 was synthesized from the tosylate precursor via two methods (A and B), as shown in Figure 1.

Method A (Tetrabutylammonium). This method of ^{18}F-PF-05270430 radiosynthesis was reported previously (*13*).

Method B (Kryptofix-222). Radiosynthesis was carried out on the TRACERLab[TM] FX$_{FN}$ automated synthesis module (GE Medical Systems, Milwaukee, WI). ^{18}F-Fluoride was produced via the [18]O(p, n)[18]F nuclear reaction by bombarding ^{18}O-water with a proton beam using the GE PETtrace cyclotron, and delivered to the synthesis module where it was trapped on an ^{18}F-separation ion-exchange cartridge. ^{18}F-Fluoride was then eluted from the cartridge into the reactor with 1.0-1.4 mL solution of Kryptofix-222 (10 mg) and K_2CO_3 (1-2 mg) in acetonitrile/water (1:0.4, v/v). Preparation of anhydrous ^{18}F-fluoride-Kryptofix-222 complex by azeotropic distillation with acetonitrile followed the procedure previously reported (*15*). After cooling the reactor to 60 ºC, 1.5 mg of the precursor in 0.5 mL of anhydrous *N,N*-dimethylformamide was added and the mixture heated at 110 ºC for 30 min. The reaction mixture was cooled to 60 °C, diluted with 15 mL of 1 mM HCl, and passed through a Waters C-18 Light SepPak cartridge that was pre-conditioned with 5 mL EtOH followed by 5 mL de-ionized (DI) water. The cartridge was eluted with 1.5 mL of acetonitrile/absolute ethanol (2:1, v/v) into a receiving vial containing 3.5 mL of 0.1 M ammonium formate with 0.5% acetic acid. The combined solution was then loaded

onto a Genesis C18 high performance liquid chromatography (HPLC) column (4 µm, 10 × 250 mm; Grace, Deerfield, IL) eluting at a flow rate of 5 mL/min with 33% acetonitrile and 67% of 0.1 M ammonium formate with 0.5% acetic acid (v/v). The product fraction was collected, diluted with 50 mL DI water, and passed through a second Waters C18 Light SepPak. The cartridge was rinsed with 10 mL of 1 mM HCl, dried, then eluted with 1 mL absolute ethanol (U.S. Pharmacopeia grade, USP), followed by 3 mL USP saline, into a product vial containing 7 mL of USP saline and 40 µL of 4.2% sodium bicarbonate (USP). This mixture was then passed through a membrane filter (0.22 µm) and collected in a sterile vial.

Chemical purity, radiochemical purity, and specific activity of the radiotracer were determined by analytical HPLC equipped with both a radioactivity detector and a UV detector (detection wavelength set at 254 nm) and a Gemini C18 column (5 µm, 4.6 × 250 mm) eluting at a flow rate of 1.5 mL/min with 45% acetonitrile and 55% of 0.1 M ammonium formate with 0.5% acetic acid. Identity of the radiolabeled compound was determined by co-injection with PF-05270430.

Metabolite analysis in rats

Two male Sprague–Dawley rats from Charles River (body weights of 306 and 344 grams) were briefly anesthetized (2-3% isoflurane in O_2) for tail vein injection of ^{18}F-PF-05270430 (67.1 and 69.1 MBq, respectively), then allowed to recover for tracer uptake. Rats were anesthetized again at 30 min post tracer injection and sacrificed by decapitation. The blood and striatum samples were collected and placed in pre-weighed tubes for further processing. Unchanged tracer in plasma and brain samples was measured using HPLC. Detailed procedures are described in the supplemental material.

PET imaging procedures in rhesus monkeys

PET imaging studies with ^{18}F-PF-05270430 were conducted in rhesus monkeys and consisted of two parts: Part 1. Test-retest experiments were performed with two monkeys (one male, 8.85 kg and one female, 7.0 kg) to determine the reproducibility of binding parameters measured with ^{18}F-PF-05270430; Part 2. Blocking experiments were conducted to assess the binding specificity of the radiotracer.

Animals were immobilized with ketamine (10 mg/kg intramuscularly) and anesthetized with 1–2% isoflurane in oxygen. PET imaging was performed on a Focus220 scanner (Siemens Medical Solutions, Knoxville, TN, USA). A 9-min transmission scan was obtained before radiotracer injection for attenuation correction. Emission data were collected in list mode for 120 or 180 min and reformatted into 33 or 45 successive frames of increasing duration (6 x 10 s, 3 x 1 min, 2 x 2 min, 22 (34) x 5 min).

Metabolite analysis and generation of input functions. The arterial input functions were generated for all scans. Arterial blood samples were drawn at 3, 8, 15, 30, 60, 90 and 120 min after tracer injection for analysis of unmetabolized fraction of the tracer using the column switching HPLC method (*16*). Detailed procedures are described in the supplemental material. The final plasma input function was calculated as the product of the total plasma activity curve and the parent fraction curve.

Measurement of plasma free fraction. An ultrafiltration-based method was used for measuring the free fraction (f_p) of ^{18}F-PF-05270430 in plasma, as described previously (*17*).

Test-retest study. Each monkey underwent two PET scans on separate days. ^{18}F-PF-05270430 was administered intravenously over 3 min by an infusion pump. Emission data were acquired for 180 min. Dynamic images were reconstructed with a filtered back projection algorithm. Regions of interest (ROIs) were manually delineated on a single representative anatomical rhesus monkey magnetic resonance image (MRI) registered to a template image.

Regions used in this study were putamen, caudate, nucleus accumbens, cingulate cortex, frontal cortex, temporal cortex, occipital cortex, and cerebellum. Registration parameters were obtained to apply the ROIs to individual PET scans, and regional time-activity curves (TACs) were generated for the ROIs.

Values of regional distribution volume (V_T) and binding potential (BP_{ND}) were computed using one-tissue (1T) and two-tissue (2T) compartment models ([18]), as well as the multilinear analysis-1 (MA1) method ([19]). For MA1, data were fitted starting at time $t^* = 30$ min. The Simplified Reference Tissue Model (SRTM) was also used to estimate BP_{ND} using cerebellum as the reference region ([20]).

The mean and standard deviation of the percentage difference between test (T) and retest (R) scans were calculated as follows:

$$\%\text{diff} = 100 \times \frac{|R - T|}{(T + R)/2}$$

Blocking experiments. Two blocking studies with the PDE2A inhibitor PF-05180999 ([11]) were performed in two different animals with 120 min of scan after injection of ^{18}F-PF-05270430. Doses of 0.2 and 2.0 mg/kg PF-05180999 were administered subcutaneously 90 min prior to tracer injection. Venous blood samples were collected at 0, 60, 90, 120, 150, and 180 min post injection to measure plasma drug exposure (see supplemental materials for detailed analysis procedures). For each study, radiotracer concentrations were measured in the same ROIs as the test-retest study.

Regional V_T and BP_{ND} values were calculated using MA1 (t^*=30 min) and SRTM. The percent change between control (C) and blocking (B) scans was computed as follows:

$$\%\text{diff} = 100 \times \frac{C - B}{C}$$

Target occupancy study in cynomolgus monkeys

Two male cynomolgus monkeys (5-6 years old) were used. For each monkey, a baseline PET scan and blocking scans with various doses of PF-05180999 (0.2, 0.4, 0.5, 0.6 and 2.0 mg/kg) were performed. PF-05180999 was administered subcutaneously 1 h prior to ^{18}F-PF-05270430 injection. Dynamic PET scans of 90 min were conducted on a Focus220 scanner. Methods on PET scanning and BP_{ND} calculation were described previously (*13*). Blood samples were collected via the jugular vein at 0, 45 and 90 min after ^{18}F-PF-05270430 injection to measure the plasma concentration of PF-05180999 during the PET scan period (see supplemental materials for details).

PDE2A target occupancy (TO) by PF-05180999 was calculated as the percentage difference in BP_{ND} between the baseline and blocking scans. The TO values in putamen and caudate were averaged to give the whole striatal occupancy. Finally, the striatal TO values from the 10 blocking scans (2 animals with 5 blocking drug doses each) were compared to the mean PF-05180999 plasma concentrations during the 90 min scan period to establish the TO versus plasma exposure relationship.

Pharmacokinetic/Pharmacodynamic (PK/PD) analysis was performed using NONMEM (NONMEM software system, version VI, GloboMax LLC, Hanover, MD, USA). A sigmoid E_{max} model (*21*) was used to correlate TO to observed plasma drug concentrations.

RESULTS

Radiosynthesis of ^{18}F-PF-05270430

When radiosynthesis Method A was applied, 3034 ± 407 MBq of ^{18}F-PF-05270430 was obtained from 76 ± 5 GBq of ^{18}F-fluoride in 81 min from end of bombardment (8.0 ± 1.7% decay-corrected yield, n=3). Radiochemical purity was >99%, with specific activity of 405 ± 14 MBq/nmol at the end of synthesis (EOS). With Method B, DMF was used as reaction solvent, and radiolabeling was carried out for 30 min at 110 °C as in Method A, except that Kryptofix-222/K_2CO_3 was used, yielding 3053 ± 901 MBq of ^{18}F-PF-05270430 from 74.4 ± 17.7 GBq of

[18]F-fluoride in 127 ± 11 min from end of bombardment. Radiochemical yield was 4.2 ±1.3 % (decay-corrected, n=19). Radiochemical purity of the final product was >98%, with specific activity of 115.2 ± 76.7 MBq/nmol (EOS).

Metabolite study in rats

Limited metabolism studies were performed in rats at 30 min post tracer injection to determine if any radioactive metabolites entered the brain. The results showed that even though only 30% and 46% of ^{18}F-PF-05270430 remained in the plasma of two rats after 30 min, majority of the radioactivity in the striatum (93% and 95%, respectively) was associated with the parent tracer (for more detail see supplemental materials).

PET imaging studies in rhesus monkeys

Test-Retest Study. The activity dose of ^{18}F-PF-05270430 was 166 ± 18 MBq, with specific activity of 69 ± 40 MBq/nmol at time of injection (n = 4).

Metabolism rate of ^{18}F-PF-0527430 was different between monkeys, but consistent between test and retest scans in the same animal (Fig. 2A). Parent fractions at 30 min after radiotracer injection were 71 ± 0.6 % for subject TM762 and 35 ± 0.3 % for BM090. Free fraction in the plasma was 20 ± 4% (*n* = 4), and not different between animals.

In the brain, distribution of ^{18}F-PF-05270430 was heterogeneous, with high uptake in the putamen and caudate and low uptake in other regions (Fig. 3A). ^{18}F-PF-05270430 displayed fast uptake kinetics, with activity levels peaked at ~7 min, followed by a rapid clearance in all brain regions (Fig. 3B).

Fitting of regional TACs by the 2T model was better than the 1T model. However, the 2T model either produced implausible parameters or did not converge in some regions. Excluding such regions, analysis by the MA1 method produced results consistent with those from 2T and

there was excellent agreement in V_T and BP_{ND} values estimated by MA1 and 2T. Values of BP_{ND} derived from SRTM were well correlated with those from 2T, but with a slope somewhat skewed from the line of identity. Given the quality of fit and comparison with BP_{ND} values estimated from 2T, MA1 was selected as the method of choice for analysis.

Distribution volumes computed with 120 min of scan data was similar to those with 180 min data ($V_{T\ 120\ min} = 1.02\ V_{T\ 180\ min} - 0.07$, $R^2=1.00$). Therefore, 120 min of the scan data were used for calculating outcome measures.

Mean V_T and BP_{ND} values obtained with MA1 and SRTM are shown in Table 1. V_T values were highest in the striatum, intermediate in the neocortical regions, and lowest in the cerebellum. Coefficient of variation (COV) was 2-6% for V_T. In the high-binding regions (putamen, caudate, and nucleus accumbens), COV was 12-13% for MA1 BP_{ND} and 12-14% for SRTM BP_{ND}. Higher COV was observed in the neocortical regions due to their low BP_{ND} values (0.05-0.5).

The test-retest variability across subjects is shown in Table 2. The V_T test-retest variability was small across all regions, while BP_{ND} variability was low in high-binding regions, and higher in low-binding regions, as expected. Test-retest variability of $V_{T\ MA1}$, $BP_{ND\ MA1}$, and $BP_{ND\ SRTM}$ was 4 ± 6 %, 13 ± 6 %, and 13 ± 7 %, respectively, in high-binding regions.

Blocking experiments. Metabolism rate of ^{18}F-PF-05270430 in blocking studies with PF-05180999 was similar to that of the baseline scans (Fig. 2B). Free fraction displayed no significant difference between baseline ($f_p = 19.5 \pm 0.4\%$, n = 2) and blocking scans ($f_p = 19.6 \pm 0.5\%$, n = 2). Inter-animal differences in metabolism were noted, however, as reinforced by the result from a baseline scan in a third animal (WM688, Fig. 2B).

Pretreatment with 0.2 mg/kg PF-05180999 did not show an obvious blocking effect (4% reduction in striatum BP_{ND}), while a dose of 2.0 mg/kg led to a significant decrease in striatum binding (73% reduction in BP_{ND}).

For blocking studies with PF-05180999, V_T in the cerebellum increased by 20-30%. The percent reduction in BP_{ND} derived from MA1 was extremely close to that from SRTM analysis. In high-binding regions, decreases in BP_{ND} (SRTM) were $3 \pm 10\%$ and $72 \pm 3\%$, respectively, for PF-05180999 doses of 0.2 mg/kg and 2.0 mg/kg. These results are summarized in Supplemental Table S2.

Target occupancy in cynomolgus monkeys

Parts of the results (representative baseline images and TACs) from the cynomolgus monkey study were presented previously (*13*). Imaging experiments with ^{18}F-PF-05270430 in cynomolgus monkeys demonstrated uptake kinetics and blocking effects similar to those in rhesus monkeys, but brain uptake levels were higher in cynomolgus monkeys (Fig. 4). Dose-dependent blockade of ^{18}F-PF-05270430 binding by PF-05180999 was seen (Supplemental Table S3). The relationship between the plasma concentration of PF-05180999 and striatum TO is plotted in Figure 5. The ten blocking scans (2 animals with 5 blocking drug doses) resulted in a range of striatum TO values from 3% to 72%, which were consistent with the mean PF-05180999 plasma exposure (40.2-240.0 ng/mL). Based on fitted sigmoid Emax model, PF-05180999 target binding EC_{50} was estimated to be 69.4 ng/mL (90% Confidence Interval: 57.9 - 80.9 ng/mL, total plasma concentration).

DISCUSSION

The identification, synthesis and PET imaging characteristics of ^{18}F-PF-05270430 has been described briefly in a previous report (*13*). In the current study we present a comprehensive characterization of this novel radioligand.

The radiosynthesis of ^{18}F-PF-05270430 involved nucleophilic displacement of the tosyl group in the azetidine ring of the precursor with ^{18}F-fluoride (Fig. 1). Direct nucleophilic

fluorination of 4-membered ring substrates is rare, and to our knowledge, this is the first example of an F-18 labeled azetidine ring in the literature. Radiofluorination in t-amyl alcohol as a solvent (Method A) in the presence of quaternary ammonium salt produced ^{18}F-PF-05270430 in higher yield than the traditional radiolabeling in polar aprotic solvents (Method B) in the presence of Kryptofix-222/K_2CO_3. Additionally, radiofluorination in t-amyl alcohol did not require extra time (~ 30 min) prior to radiolabeling in order to activate and dry the ^{18}F-fluoride by removing trace amount of water via azeotropic distillation.

Radioactive metabolite analysis in plasma showed comparable results in rats (38 ± 11% of parent at 30 min) and NHPs (35-72% at 30 min). Analysis of radioactivity in rat striatum indicated that majority of the radioactive metabolites did not get into the brain.

^{18}F-PF-05270430 displayed similar uptake pattern in the brain of rhesus and cynomolgus monkeys. In both species, it demonstrated fast uptake kinetics, with peak activity levels at 5-7 min, which was then followed by a rapid washout from all brain regions. Highest uptake levels were found in the putamen and caudate, intermediate levels in cortical regions and the lowest in cerebellum. Higher peak uptake levels were found in cynomolgus monkeys, which could be due to either higher PDE2A levels in the brain, or slower metabolism of the ligand in plasma. However, the exact reason is not known at this time, because metabolite analysis was not performed in PET scans with cynomolgus monkeys.

In rhesus monkeys, the MA1 method with 120 min of scan data returned stable measurements of regional V_T and BP_{ND} for ^{18}F-PF-05270430. SRTM analysis also gave regional BP_{ND} values well correlated with those from MA1. The test-retest variability of binding parameters derived from both methods was good (average of ~4% in V_T and ~13% in BP_{ND}). Hence, SRTM was used in the target occupancy study in cynomolgus monkeys.

The cerebellum was used as a reference region, as it had the lowest V_T. However, blocking studies with 0.2 and 2.0 mg/kg of PF-05180999 in rhesus monkey showed 22% and 28% increase, respectively, in MA1 cerebellum V_T, which was larger than the test/retest

variability of cerebellum V_T. It should be noted, however, that the percent blockade of specific binding estimated from SRTM BP_{ND} was consistent with that derived from MA1. Nonetheless, further investigation is needed to determine whether cerebellum may be used as an appropriate reference region in the analysis of ^{18}F-PF-05270430 binding parameters.

^{18}F-PF-05270430 was used to successfully measure the relationship between the plasma concentration of the PDE2A inhibitor PF-05180999 and its target occupancy in cynomolgus monkeys. Drug occupancy studies provide critical information on target engagement of therapeutic agents, which is considered one of the key factors related to the survival rate of drug candidates in clinical trials (22). Once ^{18}F-PF-05270430 is fully validated in human subjects to measure the exposure-target occupancy relationship of PDE2A inhibitors, it can provide valuable information for the selection of optimal doses in efficacy studies of drug candidates for treating schizophrenia patients.

CONCLUSIONS

In this study we have demonstrated that ^{18}F-PF-05270430 possesses fast kinetics in non-human primate brain and can be used to quantify PDE2A binding sites *in vivo* and measure target occupancy of a PDA2A inhibitor. Based on its favorable imaging properties, this novel PDE2A PET ligand has been advanced to further evaluation in humans. Results from the human study are described in the companion paper (14).

ACKNOWLEDGEMENT

REFERENCES

1.	Eaton WW, Chen CY. Epidemiology. In: Leiberman JA, Stroup TS, Perkins DO, eds. *Textbook of Schizophrenia*. Washington D.C.: American Pschiatric Publishing; 2006:17-37.

2.	Javitt DC, Laruelle M. Neurochemical Theory. In: Lieberman JA, Stroup TS, Perkins DO, eds. *Textbook of Schizophrenia*. Washington DC: American Psychiatric Publishing; 2006:85-116.

3.	Keefe RS, Harvey PD. Cognitive impairment in schizophrenia. *Handb Exp Pharmacol.* 2012;213:11-37.

4.	Keefe RS, Bilder RM, Davis SM, et al. Neurocognitive effects of antipsychotic medications in patients with chronic schizophrenia in the CATIE Trial. *Arch Gen Psychiatry.* 2007;64:633-647.

5.	Stroup TS, Kraus JE, Marder SR. Pharmacotherapies. In: Lieberman JA, Stroup TS, Perkins DO, eds. *Textbook of Schizophrenia*. Washington D.C.: American Psychiatric Publishing; 2006:303-325.

6.	Stephenson DT, Coskran TM, Wilhelms MB, et al. Immunohistochemical localization of phosphodiesterase 2A in multiple mammalian species. *J Histochem Cytochem.* 2009;57:933-949.

7.	Perez-Costas E, Melendez-Ferro M, Roberts RC. Basal ganglia pathology in schizophrenia: dopamine connections and anomalies. *J Neurochem.* 2010;113:287-302.

8.	Coyle JT. Glutamate and schizophrenia: beyond the dopamine hypothesis. *Cell Mol Neurobiol.* 2006;26:365-384.

9.	Goff DC, Coyle JT. The emerging role of glutamate in the pathophysiology and treatment of schizophrenia. *Am J Psychiatry.* 2001;158:1367-1377.

10.	Boess FG, Hendrix M, van der Staay FJ, et al. Inhibition of phosphodiesterase 2 increases neuronal cGMP, synaptic plasticity and memory performance. *Neuropharmacology.* 2004;47:1081-1092.

11.	Helal CJ, Chappie TA, Humphrey JM, Verhoest PR, Yang E. Preparation of imidazo[5,1-f][1,2,4]triazines for the treatment of neurological disorders. US patent 20120214791A1, 2012.

12.	Schroder S, Wenzel B, Deuther-Conrad W, et al. Synthesis, ^{18}F-radiolabelling and biological characterization of novel fluoroalkylated triazine derivatives for in vivo imaging of phosphodiesterase 2A in brain via positron emission tomography. *Molecules.* 2015;20:9591-9615.

13.	Zhang L, Villalobos A, Beck EM, et al. Design and selection parameters to accelerate the discovery of novel central nervous system positron emission tomography (PET) ligands and their application in the development of a novel phosphodiesterase 2A PET ligand. *J Med Chem.* 2013;56:4568-4579.

14. Naganawa M, Waterhouse RN, Nabulsi N, et al. First in human assessment of the novel PDE2A PET radiotracer ^{18}F-PF-05270430. *J Nucl Med.* 2016:In press.

15. Lim K, Labaree D, Li S, Huang Y. Preparation of the metabotropic glutamate receptor 5 (mGluR5) PET tracer [^{18}F]FPEB for human use: An automated radiosynthesis and a novel one-pot synthesis of its radiolabeling precursor. *Appl Radiat Isot.* 2014;94:349-354.

16. Hilton J, Yokoi F, Dannals RF, Ravert HT, Szabo Z, Wong DF. Column-switching HPLC for the analysis of plasma in PET imaging studies. *Nucl Med Biol.* 2000;27:627-630.

17. Gandelman MS, Baldwin RM, Zoghbi SS, Zea-Ponce Y, Innis RB. Evaluation of ultrafiltration for the free-fraction determination of single photon emission computed tomography (SPECT) radiotracers: beta-CIT, IBF, and iomazenil. *J Pharm Sci.* 1994;83:1014-1019.

18. Innis RB, Cunningham VJ, Delforge J, et al. Consensus nomenclature for in vivo imaging of reversibly binding radioligands. *J Cereb Blood Flow Metab.* 2007;27:1533-1539.

19. Ichise M, Toyama H, Innis RB, Carson RE. Strategies to improve neuroreceptor parameter estimation by linear regression analysis. *J Cereb Blood Flow Metab.* 2002;22:1271-1281.

20. Lammertsma AA, Hume SP. Simplified reference tissue model for PET receptor studies. *Neuroimage.* 1996;4:153-158.

21. Thomas N. Hypothesis testing and Bayesian estimation using a sigmoid Emax model applied to sparse dose-response designs. *J Biopharm Stat.* 2006;16:657-677.

22. Morgan P, Van Der Graaf PH, Arrowsmith J, et al. Can the flow of medicines be improved? Fundamental pharmacokinetic and pharmacological principles toward improving Phase II survival. *Drug Discov Today.* 2012;17:419-424.
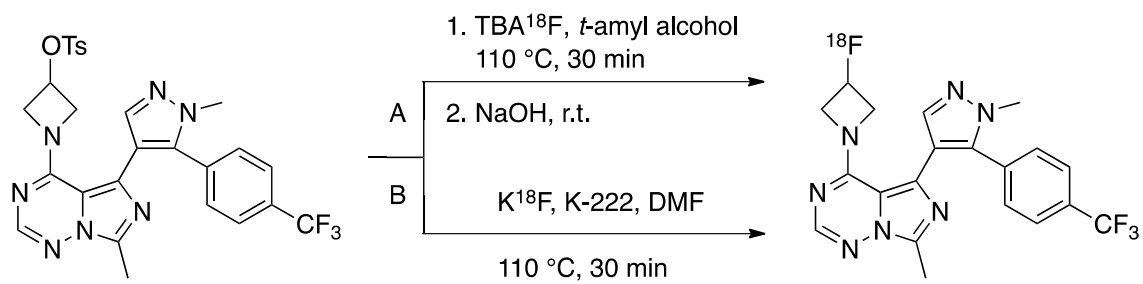
Figures

Figure 1. Radiosynthesis of ^{18}F-PF-05270430 with two methods (A and B).
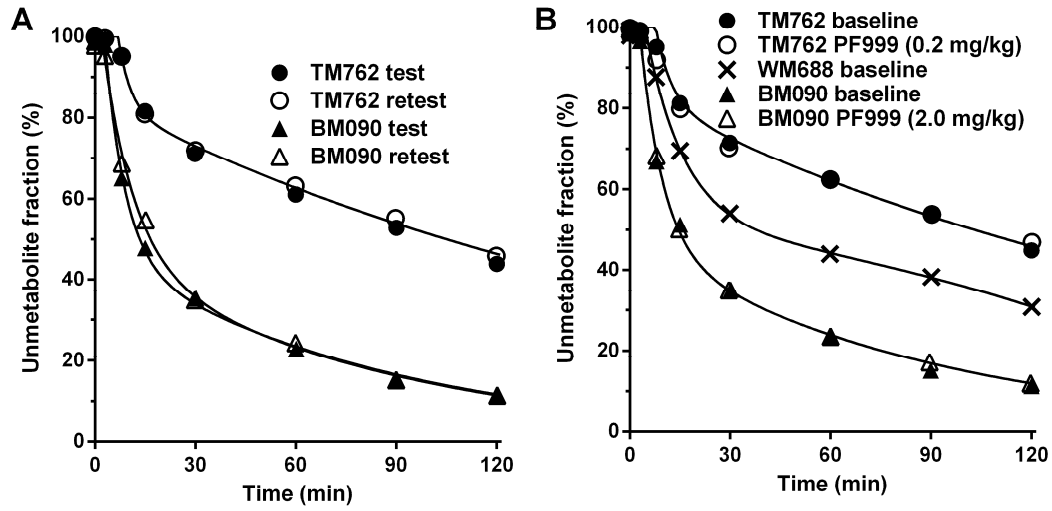
Figure 2. Unmetabolized ^{18}F-PF-05270430 fraction in plasma over time in the test-retest study (A) and in the baseline-blocking study (B) in rhesus monkeys. In B, WM688 is a 3rd monkey undergoing a baseline scan only.
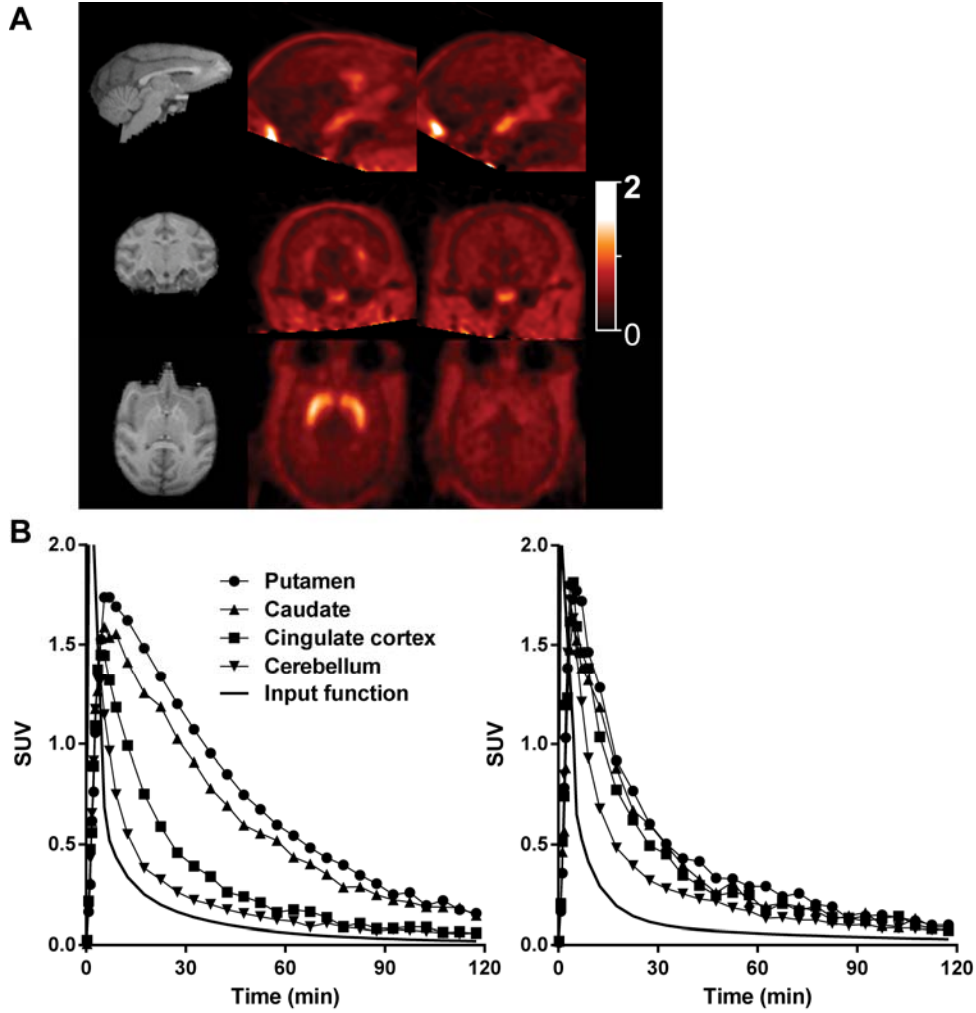
Figure 3. A. ^{18}F-PF-05270430 standardized uptake value (SUV) images from a baseline scan (middle column) and blocking scan (right column) with PF-05180999 (2.0 mg/kg) in rhesus monkey. Co-registered MRI slices (left column) are also displayed. B. Corresponding time-activity curves from the baseline (left) and blocking (right) scans.
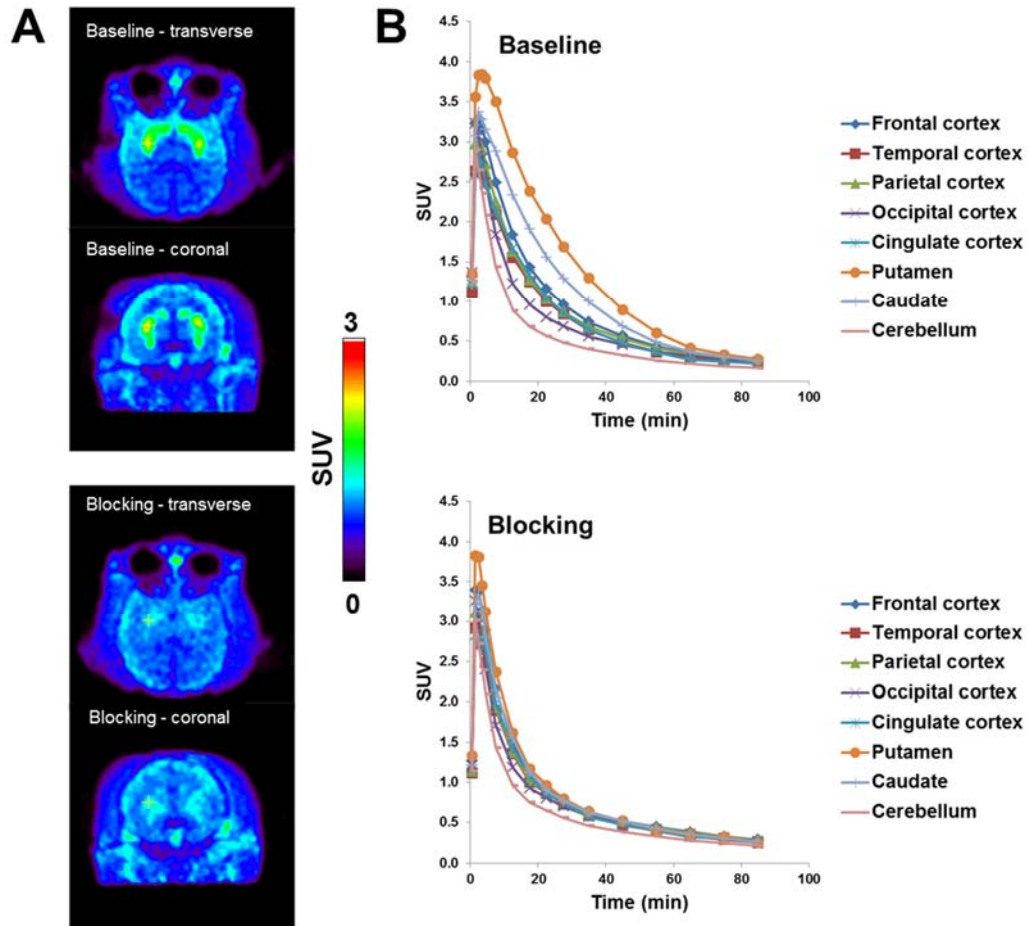
Figure 4. A. ^{18}F-PF-05270430 images in cynomolgus monkey brain summed from 0 to 60 min post-injection for the baseline (top two images) and blocking (bottom two images, 2.0 mg/kg PF-05180999 dose) scans.   B. Corresponding time-activity curves of ^{18}F-PF-05270430 under baseline (top) and blocking (bottom) conditions.
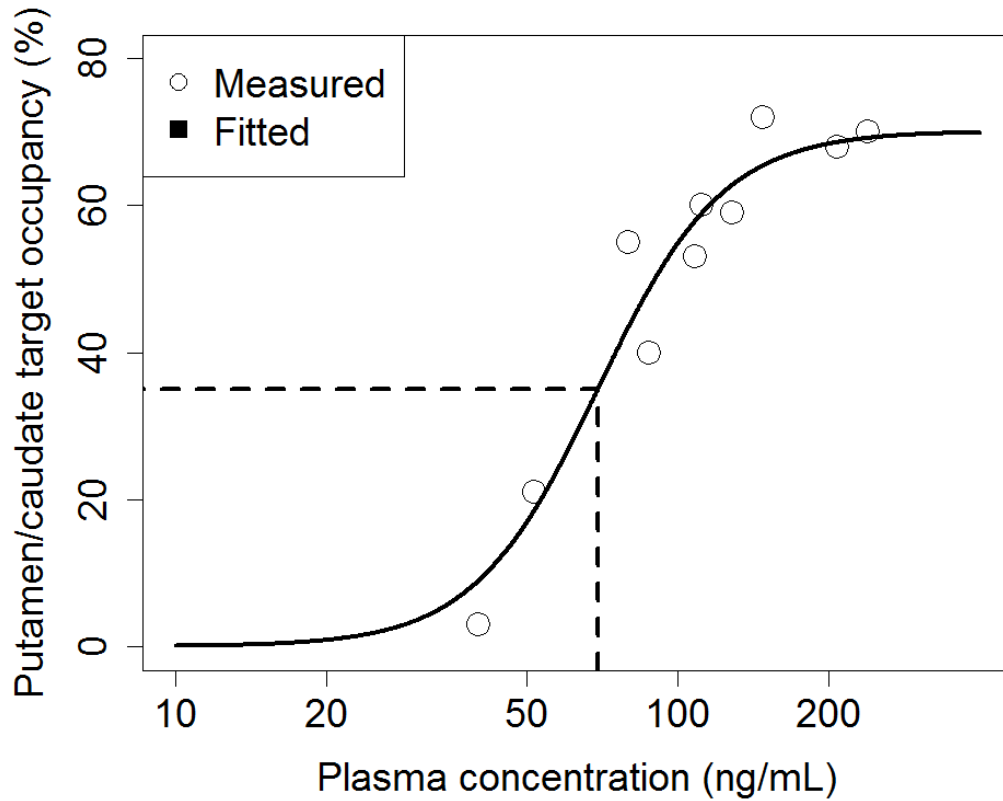
Figure 5. Relationship between PF-05180999 plasma concentration and striatum PDE2A

occupancy in cynomolgus monkeys. Open circles represent measured values and solid

curve is fitted from the sigmoid Emax model.

Tables

Table 1. Outcome measures derived from MA1 and SRTM analysis of ^{18}F-PF-05270430

imaging data in rhesus monkeys*

Region	V_T (MA1)		BP_{ND} (MA1)		BP_{ND} (SRTM)	
	Mean	COV	Mean	COV	Mean	COV
Cerebellum	1.28	6%	0	-	0	-
Occipital cortex	1.34	4%	0.05	50%	**0.06	**33%
Temporal cortex	1.59	2%	0.25	24%	0.25	29%
Cingulate cortex	1.82	5%	0.42	6%	0.44	8%
Frontal cortex	1.93	5%	0.51	18%	0.50	20%
Caudate	3.23	3%	1.54	12%	1.56	12%
Nucleus accumbens	3.42	5%	1.68	12%	1.69	13%
Putamen	3.71	3%	1.92	13%	1.96	14%

* Values of V_T and BP_{ND} averaged across four subjects.
** The mean and COV of BP_{ND} (SRTM) in the occipital cortex calculated from a single monkey (BM090, $n = 2$), because the estimates in TM762 were unstable (relative standard error > 100%).

Table 2. Test-retest variability of ^{18}F-PF-05270430 binding parameters in rhesus monkeys*

Region	% Difference between test and retest scan					
	V_T (MA1)		BP_{ND} (MA1)		BP_{ND} (SRTM)	
	Mean	SD	Mean	SD	Mean	SD
Cerebellum	4	2	-	-	-	-
Occipital cortex	4	2	61	17	**47	**-
Temporal cortex	1	1	25	5	26	6
Cingulate cortex	2	2	9	6	8	11
Frontal cortex	6	6	24	19	24	24
Caudate	4	4	11	6	11	9
Putamen	4	3	10	5	10	5
Nucleus accumbens	7	7	18	7	19	9
High-binding region	**4**	**6**	**13**	**6**	**13**	**7**

* % difference in V_T and BP_{ND} estimated from MA1 and SRTM analysis averaged across two subjects. High binding regions: putamen, caudate and nucleus accumbens.
** Test-retest variability of BP_{ND} (SRTM) in the occipital cortex calculated from a single subject (BM090), because the estimates from subject TM762 were unstable (relative standard error > 100%).